Hindawi Publishing Corporation
Advances in Mechanical Engineering
Volume 2014, Article ID 429637, 10 pages
http://dx.doi.org/10.1155/2014/429637

Research Article

Thermomechanical Fatigue Life Prediction for a Marine Diesel Engine Piston considering Ring Dynamics

Tao He,[1,2] Xiqun Lu,[1] Dequan Zou,[1,2] Yibin Guo,[1] Wanyou Li,[1] and Minli Huang[3]

[1] *College of Power and Energy Engineering, Harbin Engineering University, Harbin, Heilongjiang 150001, China*
[2] *Washington University in St. Louis, St. Louis, MO 63108, USA*
[3] *Parks College of Engineering, Aviation and Technology, Saint Louis University, St. Louis, MO 63105, USA*

Correspondence should be addressed to Xiqun Lu; luxiqun@hrbeu.edu.cn

Received 11 April 2014; Accepted 17 July 2014; Published 19 October 2014

Academic Editor: Mustafa Canakci

A newly designed marine diesel engine piston was modeled using a precise finite element analysis (FEA). The high cycle fatigue (HCF) safety factor prediction procedure designed in this study incorporated lubrication, thermal, and structure analysis. The piston ring dynamics calculation determined the predicted thickness of lubrication oil film. The film thickness influenced the calculated magnitude of the heat transfer coefficient (HTC) used in the thermal loads analysis. Moreover, the gas pressure of ring lands and ring grooves used in mechanical analysis is predicted based on the piston ring dynamics model.

1. Introduction

The increasing demand for high power density, low emission, and low fuel consumption engines impose many restrictions on the design of diesel engine components. The piston is one of the most challenging components in diesel engine design. Pistons are subjected to high thermal and mechanical loads. Large temperature difference between piston crowns and cooling galleries induce significant thermal loads. In addition, gas pressure and piston acceleration can develop cyclic mechanical stresses which are superimposed on earlier thermal stressed components. This cycle of thermal and mechanical stresses causes the thermomechanical fatigue that is the main cause of failure in diesel engine pistons.

In this study, the authors focus on damage caused by fatigue. This damage is created both by thermal and mechanical stresses [1]. To improve the life and reliability of pistons, a large number of fatigue tests are carried out when designing new pistons [2–4]. However, to reduce the cost and time involved in fatigue testing, many engine manufactures use FEA to predict the distribution of temperature and stress on engine components. The fast development of the numerical calculating technology has allowed FEA to become a significant tool in mechanical dynamics analysis, thermal analysis, and thermomechanical coupling analysis of new piston designs [5–8] and in thermomechanical fatigue analysis [9]. Under thermomechanical fatigue loading, piston failure may occur due to fatigue, material degradation due to environmental influence (oxidation), and creep mechanisms [10]. Thermomechanical fatigue life assessment methods can be classified as empirical methods, fracture mechanics theories, continuum mechanical models, and models based on microstructure [11]. Empirical models correlate the number of cycles to failure to parameters of the hysteresis loop, for example, stress, strain, and plastic strain [12].

In this study, a three-dimensional FEA is used to predict the thermomechanical behavior of a newly designed diesel marine engine piston. In order to accurately determine the heat transfer coefficient (HTC) of the piston head, the oil film is taken into consideration in the thermal analysis. The thicknesses of oil film between ring/piston and ring/bore are determined using a ring pack lubrication model. To calculate the oil pressure distribution in the piston lands/grooves operation, a piston ring dynamics model is used in the mechanical loads analysis. The coupled actions of thermal loads and mechanical loads (including combustion pressure, inertial load, and oil pressure in ring lands/grooves) are used to predict fatigue life. The prediction procedure designed

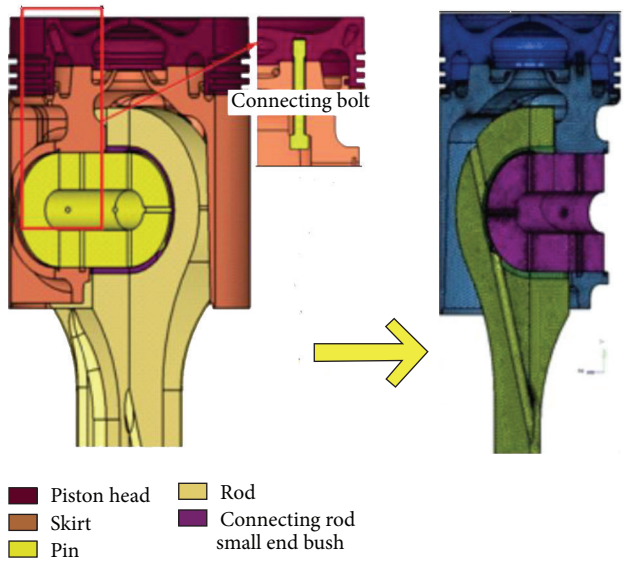

(a) Solid model of piston (b) FE model of piston

Figure 1: The solid and FE model of the piston.

Table 1: Engine parameters and piston materials.

Design structure	Composite
Diameter of bore (mm)	270
Max. combustion pressure (MPa)	23
Rated power (KW)	455
Rated speed (rpm)	1000
Stroke (mm)	330
Material of head	42CrMoA
Material of skirt	QT700-2
Material of bolt	18Cr2Ni4WA
Material of pin	12CrNi4A

in this study is the combination of lubrication analysis and structure analysis. The results obtained by this new method will provide a guideline for further optimizing piston design.

2. The Finite Element Model

Due to the symmetrical structure of the piston, a 1/4 3D solid model (Figure 1(a)) including piston, pin, and rod was created. The FE software ANSYS was used for FEA in this study. For the FE model, 3D 8-node solid elements solid45 was chosen to perform the thermomechanical coupled analysis. As shown in Figure 1(b), 37246 nodes and 60638 elements were obtained. The materials of each part are listed in Table 1. Since this study focuses on the piston properties, the connection rod is set as a rigid body for analysis.

The surface-surface contact unit is placed on the contact surface between the piston pin hole and the piston pin, head and skirt, head and bolt, skirt and bolt, pin and bush, pin and skirt, and bush and rod. Figure 2 shows the contact pairs in this piston model.

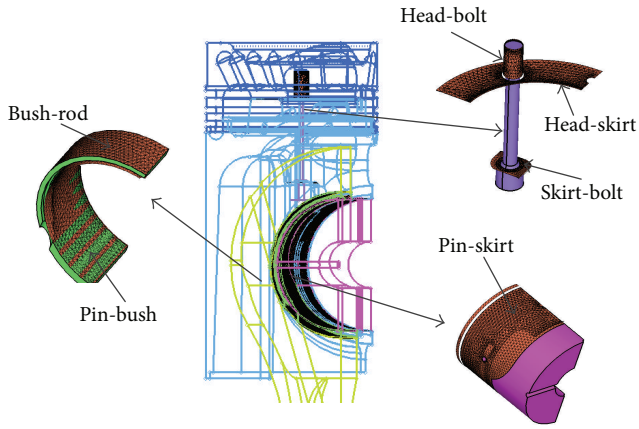

Figure 2: The contact pairs distribution in the piston model.

3. Theory

3.1. Thermal Boundary Conditions. Piston temperature is usually considered to be independent of the operating states and remains constant during a working cycle [13]. Since the time response of piston material to the variation of boundary conditions in a firing cycle is very slow, a steady state thermal analysis has been done considering the typical values of temperatures and heat transfer coefficients at piston boundary surfaces during one firing cycle. Based on the third kind of steady-state heat conduction, conductive heat transfer boundary condition is that the temperature of the fluid medium contacting to the objects and the heat transfer coefficient are known, and can be shown as

$$k\frac{\partial T}{\partial n}\bigg|_y = \alpha\left(T - T_f\right)\big|_y, \quad (1)$$

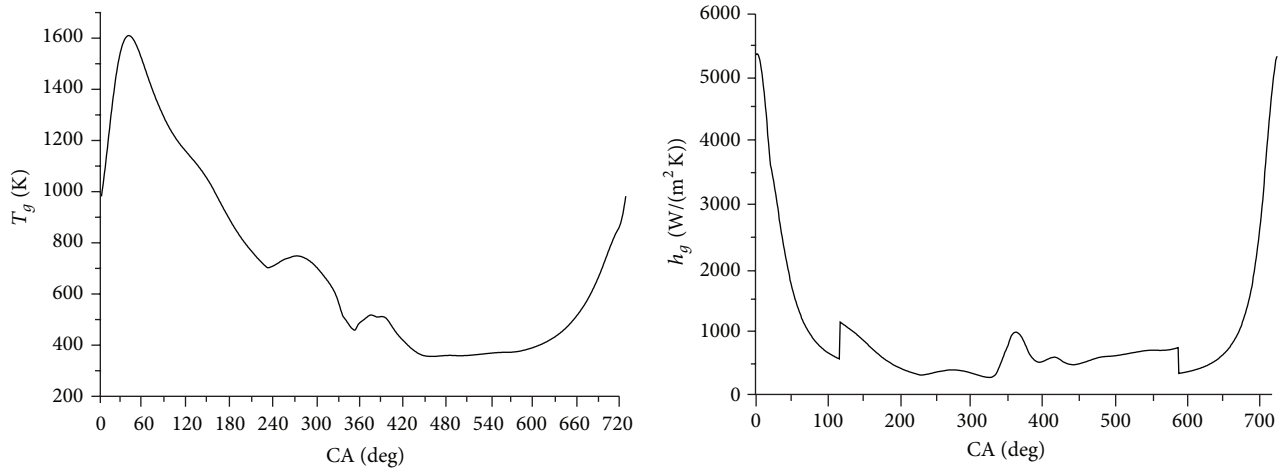

FIGURE 3: h_g, T_g calculated by GT-Power.

where T_f is the medium temperature, α is the HTC, and T_f can be constant or time and position variety, as well as α [14].

(1) HTC on Piston Top Surface. Based on the assumption of a steady working state of the engine, the average HTC and the average piston surface temperature in a whole working cycle can be given as

$$h_m = \frac{1}{720}\int_0^{720} h_g d\varphi,$$
$$T_{\text{res}} = \frac{1}{720 \cdot h_m}\int_0^{720} h_g T_g d\varphi, \tag{2}$$

where h_g, T_g are the instant HTC of gas at piston surface and instant gas temperature. According to the design parameters of the engine, h_g and T_g can be calculated by GT-Power (Figure 3). According to (2), $h_m = 1214.88\,\text{W/m}^2\,\text{K}$ and $T_{\text{res}} = 913.31\,\text{K}$.

Using Seal's formula and experimental data, the HTC of piston head is the function of position in radial direction:

$$\text{If } r < N, \quad h_r = \frac{2h_m}{1 + e^{0.1N^{1.5}}} e^{0.1r^{1.5}},$$
$$\text{If } r \geq N, \quad h_r = \frac{2h_m}{1 + e^{0.1N^{1.5}}} e^{0.1(2N-r)^{1.5}}, \tag{3}$$

where r is the distance from a local point to the center axis of the piston head and N is the distance from the point where the maximum temperature occurs to the center axis of the piston. For FEA modeling, the top surface of the piston is divided into 10 subregions radially. Then, based on the piston's structural parameters, the HTC on the top of head can be determined by (3). The HTC distribution of the top head of the newly designed piston is shown in Figure 4.

(2) HTC at Skirt and Cooling Oil Channels. The current analysis used HTC values at the skirt and oil channels that were determined by Lu et al. [14]. Their analysis used a piston with a similar structure and size.

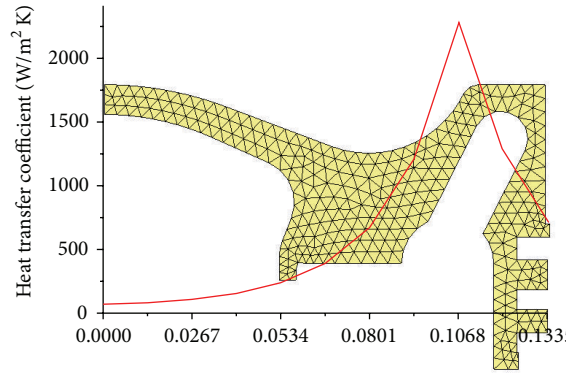

FIGURE 4: HTCs distribution at the top of piston head.

(3) HTCs at Piston Ring Lands/Groove. The thermal transfer process in piston ring lands/grooves is shown in Figure 5. Figure 5(a) is the thermal resistance map from piston to bore through ring land, and Figure 5(b) is the thermal resistance map from piston to bore through ring groove. The resistances in the transfer paths (Figure 5) have been specific by Lu et al. [15]. Parameters such as the position of ring during operation and the thickness of oil film between ring/bore and ring/piston are important in the heat transfer process. In order to predict the magnitude of those parameters, a ring dynamics analysis is applied in this study.

(4) Ring Dynamics. The motion of piston ring within the piston groove can be described by the axial rotational (torsional twist) and radial motions in the three respective degrees of freedom. The ring motion in the circumference direction is neglected in this study. A small section of the ring at a circumferential location is considered in the analysis (Figure 6). The whole ring dynamic analysis model developed by Tian et al. [16] is used in this study. Considering the complexity of heat transfer and time consumption of

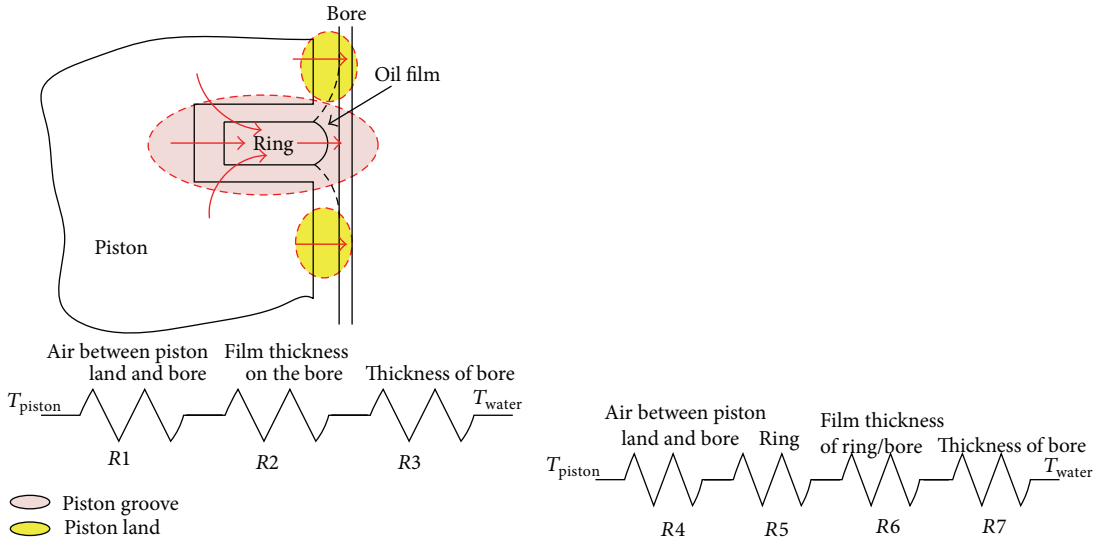

(a) Resistance map of heat transfer in piston land

(b) Resistance map of heat transfer in piston groove

Figure 5: The resistance map of heat transfer from piston head to bore.

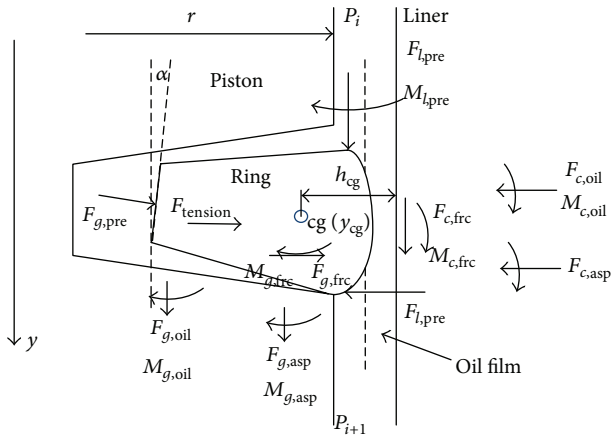

Figure 6: Free body diagram of ring cross section.

simulation, the section of thrust side (TS) is used. The governing equations for the ring motion are

$$\begin{aligned} m_r \frac{d^2 y_{cg}}{dt^2} &= F_{g,oil} + F_{g,asp} + F_{c,frc} - F_{l,pre} - m_r g, \\ I_r \frac{d^2 \alpha}{dt^2} &= M_{g,oil} + M_{g,asp} + M_{c,frc} + M_{l,pre} + M_{c,oil} \\ &\quad + M_{c,asp} - K_{rt}\alpha, \\ m_r \frac{d^2 h_{cg}}{dt^2} &= F_{g,pre} + F_{g,frc} + F_{c,oil} - F_{c,asp} \\ &\quad - F'_{l,pre} + K_{rr}\left(h' + h_0\right), \end{aligned} \tag{4}$$

where y_{cg} and h_{cg} are the axial and radial position of the center of gravity of the ring and α is the twist angle. m_r, I_r, and K_{rt} are ring mass, moment of inertia for toroidal rotation, and cross-sectional torsional stiffness. K_{rr} is the radial tension stiffness, h' is the reduction in ring radius at installation, and h_0 is the minimum ring-bore oil film thickness ($F_{tension} = K_{rr}(h' + h_0)$). F and M are the forces and moments acting on the ring cross section (Figure 6). In (4) the first subscript for the force and moment terms indicates location on the ring (g = groove, c = cylinder, and l = land) and the second subscript describes the source of the force or moment (oil = oil pressure, asp = normal pressure due to asperity contact, pre = gas pressure, and frc = hydrodynamic or boundary friction). The torsional moment M_{rt} is calculated as

$$M_{rt} = K_{rt}\alpha. \tag{5}$$

For a complete ring with rectangular cross section, the cross-sectional torsional stiffness (K_{rt}) is given by

$$K_{rt} = \frac{Eb^3 \ln(D/d)}{3(D+d)}, \tag{6}$$

where E is the modulus of elasticity of piston ring, b is the axial height of piston ring section, d is the inner diameter, and D is the outer diameter of piston ring. The axial motion of a ring relative to piston can be expressed as

$$\begin{aligned} y_{cg} &= y_p + y_{rp}, \\ \frac{dy_{cg}}{dt} &= \frac{dy_p}{dt} + \frac{dy_{rp}}{dt}, \\ \frac{d^2 y_{cg}}{dt^2} &= \frac{d^2 y_p}{dt^2} + \frac{d^2 y_{rp}}{dt^2}, \end{aligned} \tag{7}$$

where y_p is the axial position of the piston and y_{rp} is the axial position of the ring related to the piston. And y_p can be given

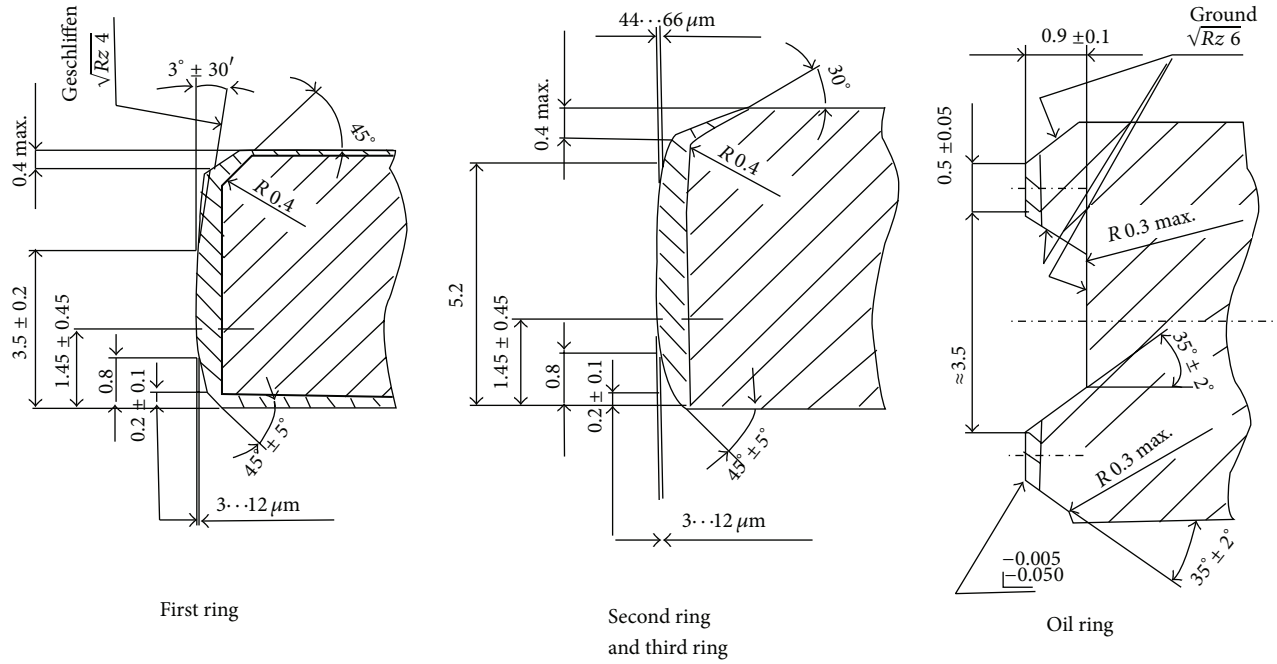

FIGURE 7: The geometry of the piston rings.

out by the piston secondary motion together with the axial motion. Using a developed version of an existing ring pack lubrication model, Gamble et al. [17] investigated the effect of piston secondary motion on the performance of a diesel engine piston ring pack, in terms of gas flow and interring gas pressures. For an example engine operating condition, the effect of secondary motion on the ring pack was calculated for a number of ring gap positional combinations. The secondary motion and the positions of the ring gaps were shown to have an effect on the ring pack operating conditions, such as oil film thickness, friction, wear, oil transport, and degradation. And in order to determine the parameter y_p, the tilt of piston and axial position are needed, and those two parameters can be calculated by iteration algorithm used in [17].

Forces and moment associated with land and groove gas pressure are calculated using pressure solutions from the gas dynamics submodel. Forces and moments associated with oil pressure are obtained from the lubrication submodel, and those associated with local asperity contact pressure are calculated by asperity deformation model. Ring axial position and twist influence gas flow paths and the forces at the ring-groove interface. Ring twist also affects the effective profile presented by the ring face to the cylinder bore and thus affects oil film thickness and ring friction. The lubrication model, asperity deformation model, and oil film squeezing model at ring side and groove interface have been previously described [16, 18].

The structure of the rings used in the piston is shown in Figure 7. Each ring is modeled as a single mass; twisting (including pretwist angles) is considered. The equations of motion, which considers equilibrium condition of moments and forces for each ring, are solved. The dynamic components of ring motion are calculated using time integration methods.

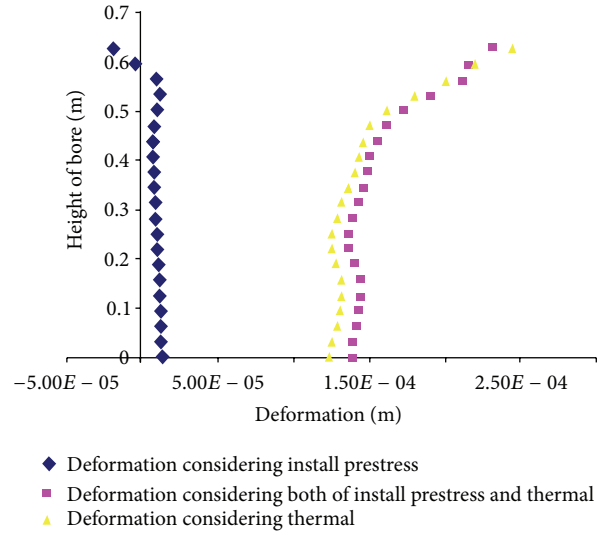

FIGURE 8: The bore deformation.

The cylinder liner typically shows a deformation along cylinder length axis and along cylinder circumference due to bolting prestress and thermal load in the real condition. In this study, the deformation of bore in different cases has been given by Figure 8. The mechanism of piston ring sealing is equivalent to a labyrinth seal, where the gap clearances are determined by the position of the rings in the groove considering the global movement and tilting of the piston [17]. The Reynolds equations are solved iteratively in each time step to determine the hydrodynamic pressure distribution between ring running surface and liner. All

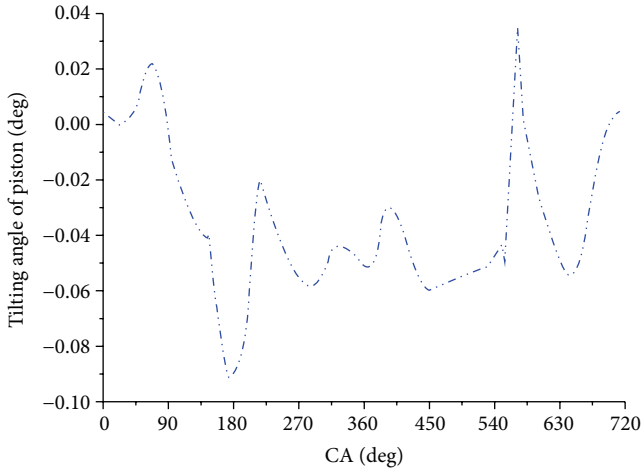

Figure 9: The tilting angle of piston during operation.

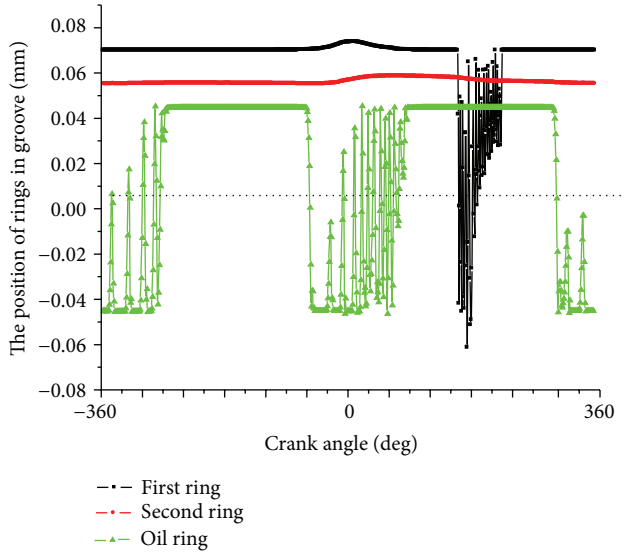

Figure 10: The position of rings in groove.

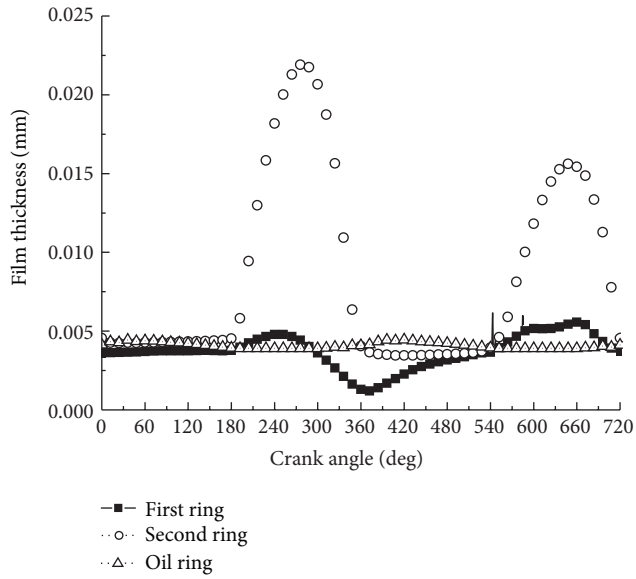

Figure 11: The film thickness of each ring.

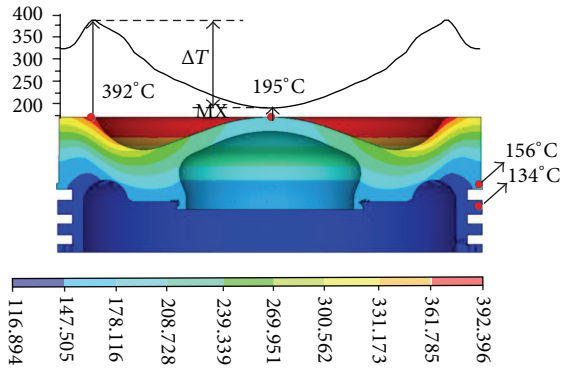

Figure 12: The temperature distribution of piston head.

relevant mechanisms are considered; the calculation is done quasi-statically per time step. The tilting angle of piston is given by Figure 9. And the motion of each ring in groove during operation is shown in Figure 10 and the thickness of film oil between each ring face and bore is shown in Figure 11.

3.2. Temperature Distribution. Using the mathematical model developed above, the HTCs distribution in piston grooves/lands can be determined after getting the position of each ring and the film thickness between each ring and bore. Based on the determined HTCs in the top head, piston lands/grooves, and piston skirt, the temperature distribution of the piston is predicted by FEA in ANSYS (Figures 12 and 13). As shown in Figures 12 and 13, the temperature intensity distribution decreases gradually from the head of the piston to the bottom of the skirt. A maximum temperature of approximately 392°C is obtained on the head of the piston at the combustion chamber chamfer edge (Figure 12). This result is similar to that obtained on a similar type of piston in an earlier study [19]. The temperature decreases radically towards the outside and inside of piston. The temperature is 156°C and 134°C at the bottom of fire land and second land, respectively. As it is shown in Figure 11, the temperature distribution in the skirt, bolt, and pin are lower than the piston. The maximum temperature is 155.6°C, 250°C, and 99.7°C, respectively.

3.3. The Mechanical Loads. The working piston not only bears a thermal load, but also the high pressure of the fuel gas and the inertia force created by the reciprocating motion. The most strenuous condition of running the piston is the moment when the pressure in the combustion chamber reaches its maximum value. Therefore, this study lays emphasis on the stable stress at the combustion moment when operating at a stable speed.

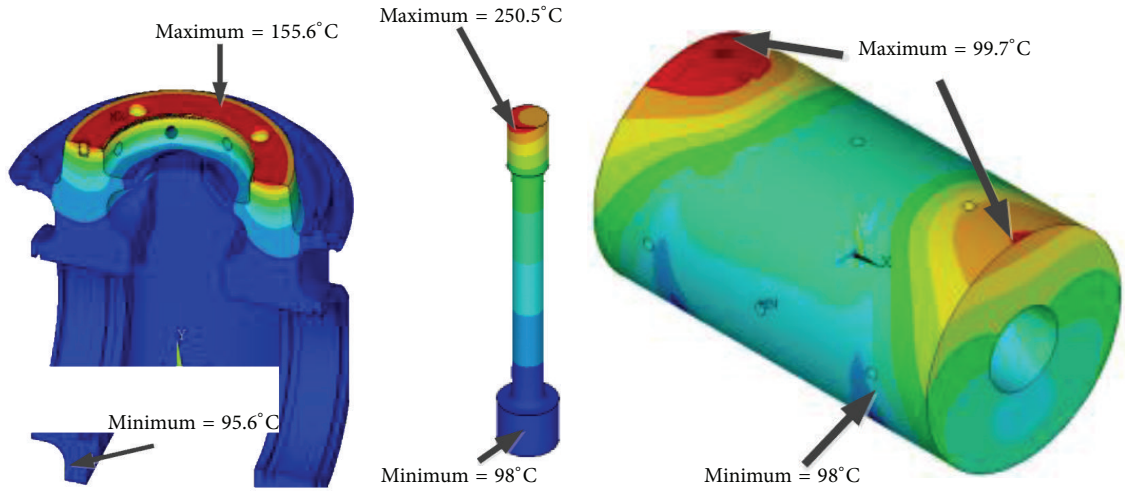

FIGURE 13: The temperature distribution of piston skirt, connect bolt, and piston pin.

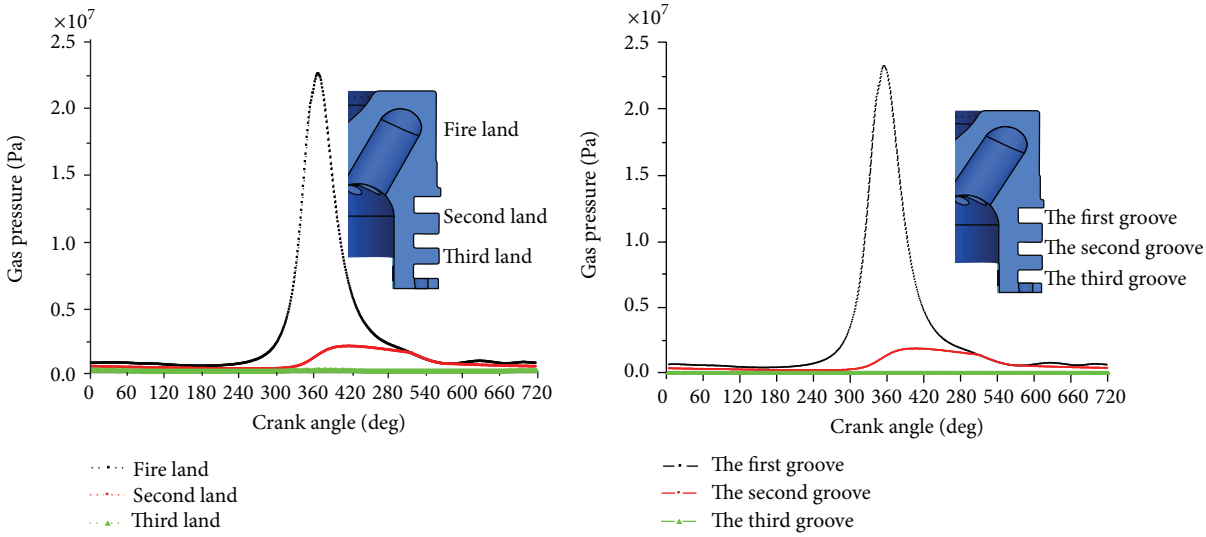

FIGURE 14: The pressure in lands and grooves versus crank angle.

(1) Gas Pressure. Gas pressure is primary loaded on the top of head. However, the piston lands and grooves are also loaded. The gas pressure in the chamber is calculated from GT-POWER based on the design parameters of the new piston. The pressure acts on ring lands and grooves are calculated using a piston ring dynamics program. Based on the ring dynamics model developed above, the gas pressure in lands and grooves are calculated (Figure 14).

(2) Reciprocating Inertial Force. Due to the reciprocating motion of piston in the cylinder, the inertial force of the piston cannot be ignored in the mechanical analysis. Based on the engine dynamics, the reciprocating inertial force P_j is related to the acceleration of the piston. The force action line is parallel to the center line of the cylinder. Because the inertial force direction is opposite to the acceleration, the effect of gas pressure on piston might be subducted. The reciprocating inertial force is calculated as

$$P_j = -m_j (1 + \lambda) R\omega^2. \quad (8)$$

The acceleration at the moment of combustion is given as

$$a = R\omega^2 (\cos\alpha + \lambda \cos 2\alpha), \quad (9)$$

where ω is the angular velocity, $\omega = n\pi/30$, n is the rotational speed, rpm, and λ is the ratio of crank radius R and rod length L.

3.4. Thermomechanical Fatigue Life Prediction. The high cycle fatigue prediction is based on the thermomechanical

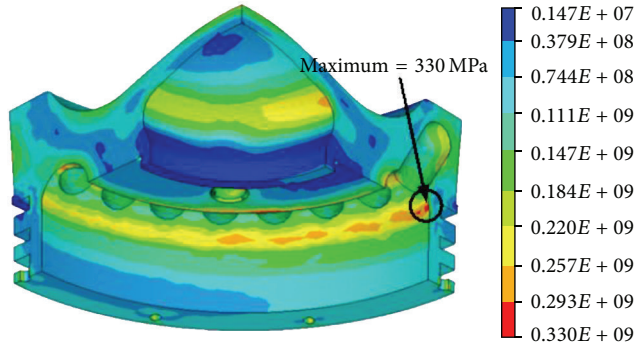

Figure 15: The von Mises stresses in piston head.

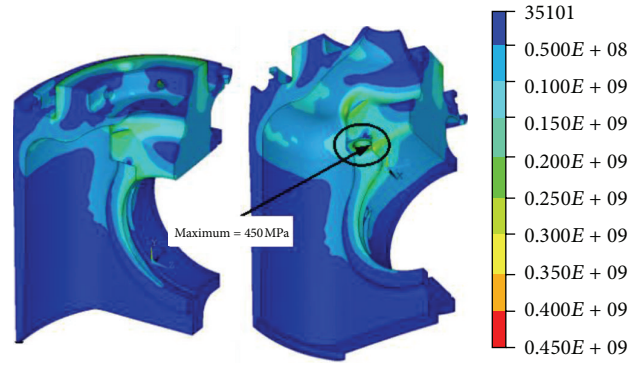

Figure 16: The von Mises stresses in piston head.

analysis results of alternating conditions. The first condition is the moment when the piston is at the top dead point after outbreak and the alternate condition is when the piston is at the bottom dead point in the exhaust stroke. The Haigh diagram is modified according to the magnitude of the stress gradient, nodal temperature, and modification factors at each node. The mean and alternating stresses resulting from the alternating conditions are computed at each node; then, the HCF safety factor for each node is attained.

The selection of the displacement boundary condition significantly affects the finite element analysis. A symmetrical restraint is applied on the symmetry plane because a quarter of a symmetric piston is modeled. Three degrees of freedom on the bottom of the rod of the piston assembly are restrained to hold the piston in a static condition.

In this analysis, a multilinear kinematic hardening model is used to account for material nonlinearity. The following load cases are defined to simulate different stages of the work cycle:

(1) application of the pretension force of the bolt to the model;

(2) application of thermal loads (temperature) to the model;

(3) application of inertia loads (piston acceleration) to the model;

(4) application of maximum pressure of combustion gases to the top head, the lands pressures, and grooves pressures to the model.

4. Results and Analysis

The distribution of equivalent von Mises stresses in the piston head after application of thermal loads, inertia loads, pressure of combustion gases, and ring region pressure is shown in Figure 15. In the cooling oil chamber closed to the first groove, the induced stresses are high, 330 MPa, due to the reduction of piston wall thickness and stress concentration effect. Figure 16 shows the distribution of equivalent von Mises stresses in the piston skirt. The areas around the contact regions of piston skirt and piston pin are subjected to severe stresses, 450 MPa (Figure 16).

The commercial software FE-SAFE is used to calculate the HCF safety factors. The contour of the HCF safety factors in the piston head and pin is shown in Figure 17. The safety factors in the piston head and pin are more than 1.8. This indicates that the design of those components can meet the life limitation. Variable tensile and compressive mean stresses are observed in different regions of the piston skirt (Figure 18). The maximum compressive mean stresses due to mechanical loads are observed in the piston pin hole (114 MPa). The maximum tensile stresses are located on the contact face between connection bolt and skirt (145 MPa).

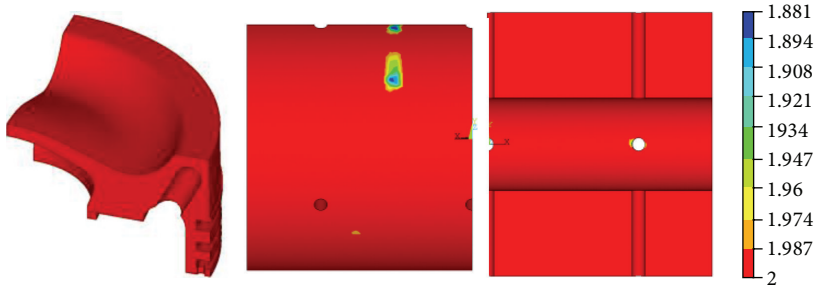

Figure 17: The safety factor distribution in head and pin.

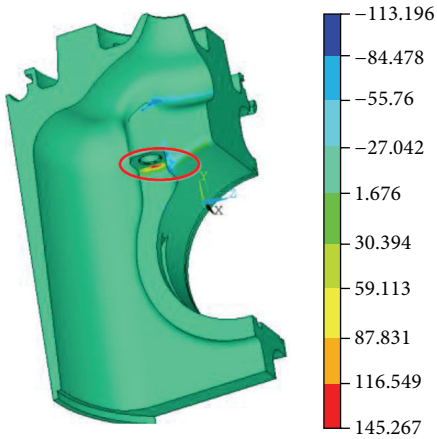

Figure 18: The mean stresses distribution in piston skirt.

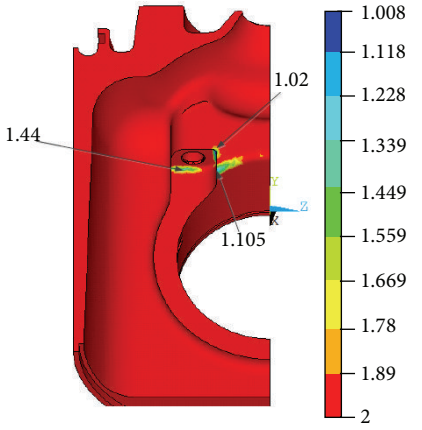

Figure 19: The safety factor distribution in piston skirt.

The safety factors at the inner contact areas of pin-pin hole and bolt-skirt are lower than other regions (Figure 19); the minimum value is just 1.02 which does not reach the strength requirement of 1.5.

5. Conclusions

This study performs a detailed thermomechanical stress analysis on a diesel engine piston. Temperature distribution is determined from thermal analysis. In order to calculate the HCF safety factor, the commerce software FE-SAFE is used. A piston ring dynamics calculation is used to determine the thickness of lubrication oil film when calculating the magnitude of the heat transfer coefficient (HTC) in thermal loads analysis. The gas pressure of ring lands and ring grooves in mechanical analysis is calculated using a piston ring dynamics model. The prediction procedure designed in this study is the combination of lubrication, thermal, and structure analysis. The results obtained using this new method provide a guideline for further optimizing the design and manufacture of new pistons. Future work will focus on experimental validation.

Conflict of Interests

The authors declare that there is no conflict of interests regarding the publication of this paper.

Acknowledgments

The present research has been funded by the National Natural Science Foundation of China (Grant no. 51375104) and the Fundamental Research Funds for the Central Universities (Code HEUCFZ1117); the authors would like to sincerely express their appreciation. And the authors greatly thank Melanie Koleini in Washington University for her assistance in checking and refining the language.

References

[1] F. S. Silva, "Fatigue on engine pistons—a compendium of case studies," *Engineering Failure Analysis*, vol. 13, no. 3, pp. 480–492, 2006.

[2] W. Zhang, C. Wei, Z. Su, J. Liu, and J. Xiang, "Study on forecasting of fatigue life for aluminum alloy piston of diesel engine," *Zhongguo Jixie Gongcheng/China Mechanical Engineering*, vol. 14, no. 10, pp. 865–867, 2003.

[3] M. T. Abbes, P. Maspeyrot, A. Bounif, and J. Frene, "A thermo-mechanical model of a direct injection diesel engine piston," *Proceedings of the Institution of Mechanical Engineers Part D*, vol. 218, no. 4, pp. 395–409, 2004.

[4] Y. Liu, Y. Wang, X. Men, and F. Lin, "An investigation on piston pin seat fatigue life on the mechanical fatigue experiments," *Key Engineering Materials*, vol. 324-325, pp. 527–530, 2006.

[5] S. Y. Liu, F. H. Lin, Y. Z. Qin, and Z. M. Wang, "Piston durability research based on the pin-bore profile design," *Chinese Internal Combustion Engine Engineering*, vol. 28, no. 1, pp. 46–50, 2007.

[6] Y. Wang, Y. Dong, and Y. Liu, "Simulation investigation on the thermo-mechanical coupling of the QT 300 piston," in *Proceedings of the 2nd International Conference on Information and Computing Science (ICIC '09)*, vol. 4, pp. 77–80, Manchester, UK, May 2009.

[7] Y. Wang, Y. Liu, and H. Shi, "Simulation and analysis of thermo-mechanical coupling load and mechanical dynamic load for a piston," in *Proceedings of the 2nd International Conference on Computer Modeling and Simulation (ICCMS '10)*, pp. 106–110, Sanya, China, January 2010.

[8] M. Ayatollahi, R. F. Mohammadi, and H. R. Chamani, "Thermo-mechanical fatigue life assessment of a diesel engine piston," *International Journal of Automotive Engineering*, vol. 1, no. 4, pp. 256–266, 2011.

[9] S. R. Lampman, *Asm Metals Handbook Volume 19—Fatigue and Fracture*, ASM International, 1997.

[10] T. Gocmez, A. Awarke, and S. Pischinger, "A new low cycle fatigue criterion for isothermal and out-of-phase thermomechanical loading," *International Journal of Fatigue*, vol. 32, no. 4, pp. 769–779, 2010.

[11] R. Minichmayr, M. Riedler, G. Winter, H. Leitner, and W. Eichlseder, "Thermo-mechanical fatigue life assessment of aluminium components using the damage rate model of Sehitoglu," *International Journal of Fatigue*, vol. 30, no. 2, pp. 298–304, 2008.

[12] M. M. Rahman, A. K. Ariffin, N. Jamaludin, S. Abdullah, and M. M. Noor, "Finite element based fatigue life prediction of a new free piston engine mounting," *Journal of Applied Sciences*, vol. 8, no. 9, pp. 1612–1621, 2008.

[13] P. Gudimetal and C. V. Gopinath, "Finite element analysis of reverse engineered internal combustion engine piston," *Asian International Journal of Science and Technology in Production and Manufacturing Engineering*, vol. 2, no. 4, pp. 85–92, 2006.

[14] X. Lu, Q. Li, W. Zhang, Y. Guo, T. He, and D. Zou, "Thermal analysis on piston of marine diesel engine," *Applied Thermal Engineering*, vol. 50, no. 1, pp. 168–176, 2013.

[15] X.-Q. Lu, T. He, D.-Q. Zou, Y.-B. Guo, and W.-Y. Li, "Thermal analysis of composite piston in marine diesel engine based on inverse evaluation method of heat transfer coefficient," *Chinese Internal Combustion Engine Engineering*, vol. 33, no. 4, pp. 71–76, 2012.

[16] T. Tian, L. B. Noordzij, V. W. Wong, and J. B. Heywood, "Modeling piston-ring dynamics, blowby, and ring-twist effects," *Journal of Engineering for Gas Turbines and Power*, vol. 120, no. 4, pp. 843–854, 1998.

[17] R. J. Gamble, M. Priest, R. J. Chittenden, and C. M. Taylor, "Preliminary study of the influence of piston secondary motion on piston ring tribology," *Tribology Series*, vol. 38, pp. 679–691, 2000.

[18] R. Keribar, Z. Dursunkaya, and M. F. Flemming, "Integrated model of ring pack performance," *Journal of Engineering for Gas Turbines and Power*, vol. 113, no. 3, pp. 382–389, 1991.

[19] D.-M. Lou, Z.-Y. Zhang, and L.-L. Wang, "Heat transfer boundary condition and thermal load of combined-piston for locomotive diesel engines," *Journal of Tongji University*, vol. 33, no. 5, pp. 664–667, 2005.